2013

Mineralogy and chemistry of late pliocene-early pleistocene palesols on Mount Kenya: weathering indices of relative age and paleoenvironmental reconstruction

Mahaney, W.C.

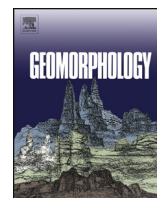Elsevier

Mineralogy and chemistry of Late Pliocene–Early Pleistocene paleosols on Mount Kenya: Weathering indices of relative age and paleoenvironmental reconstruction

W.C. Mahaney [a,b,*], T.S. Hamilton [c], R.W. Barendregt [d], R.G.V. Hancock [e,f], P. Costa [g,h]

[a] Quaternary Surveys, 26 Thornhill Ave, Thornhill, Ontario L4J1J4, Canada
[b] Department of Geography, York University, N. York, Ontario M3J 1P3, Canada
[c] Camosun College, Department of Chemistry and Geoscience, Camosun College Lansdowne Campus, 3100 Foul Bay Rd., Victoria, British Columbia V8P 5J2, Canada
[d] University of Lethbridge, Department of Geography, Lethbridge, Alberta T1K 3M4, Canada
[e] Medical Physics and Applied Radiation Sciences, McMaster University, Hamilton, Ontario L8S 4K1, Canada,
[f] Department of Anthropology, McMaster University, Hamilton, Ontario L8S 4K1, Canada
[g] University of Lisbon, Department of Geology, Lisbon, Portugal
[h] Department of Geography, Dundee University, Dundee, Scotland, UK

ARTICLE INFO

ABSTRACT

Iron and Al extracts as weathering indices in paleosols have been used in many localities to determine relative age, transformation of total chemical element concentrations to secondary forms, translocation of organically-complexed Al and long-standing inundation of soils with groundwater. On Mt. Kenya, a succession of paleosols straddling the Olduvai subchron are here analyzed to determine the degree to which Fe/Al extracts assist paleoenvironmental reconstruction, especially relative age determination, genesis and translocation of alteration products and the effect of paleoclimatic deterioration with the advent of glaciation ca. 2.0 Ma, and possibly before. Warmer/humid climate from the onset of the Plio-Pleistocene to the Olduvai subchron, thereafter reverting to a long episode of oscillating drier/wetter ice age perturbations is written into the profile morphologies, mineralogies and chemistries supporting earlier stratigraphic interpretations.

© 2013 Elsevier B.V. All rights reserved.

1. Introduction

Iron and Al extracts have been used in a number of different latitude belts, on a range of lithologies from equator to pole to reconstruct pedogenic trends related to time and climate (Blume and Schwertmann, 1969; Alexander, 1974; Parfitt and Childs, 1988; Mahaney et al., 1991, 1999; Pai et al., 2004; Mahaney et al., 2006; Schülli-Maurer et al., 2007; Mahaney et al., 2009, 2010, 2012). Over the last four decades, three extracts of Fe and Al including Na-pyrophosphate (Fe_p/Al_p), acid ammonium oxalate (Fe_o/Al_o) and Na-dithionite (Fe_d/Al_d), each have been taken from stratigraphically important suites of soils/paleosols to determine relative age, translocation of organic carbon, reduction in lattice Fe with weathering and relative increases in secondary hematite plus goethite. Originally it was thought that Fe_p approximated organically-complexed Fe (McKeague and Day, 1966), a relationship later shown to be in error (Parfitt and Childs, 1988). Na-pyrophosphate extracts of Al (Al_p), long considered an approximation of organically-complexed Al, have been shown (Parfitt and Childs, 1988; Mahaney et al., 2009) to be an accurate proxy for organic carbon translocation in a variety of different environments. Acid ammonium oxalate extracts of both Fe_o and Al_o, originally considered to represent amorphous forms of both elements, are now known to approximate the concentration of ferrihydrite ($5Fe_2O_3.9H_2O$) in paleosols (Parfitt and Childs, 1988). Walker (1983) asserted that soils with high magnetite concentrations are prone to erroneously elevated values of Fe_o due to oxalate–magnetite interactions; however, as discussed later, samples here with high concentrations of magnetite, do not show anomalous values. The Al_o concentration represents a mass of secondary Al products (Mahaney and Fahey, 1988; Birkeland et al., 1989; Mahaney et al., 2009), which when compared with Al_p ($Al_o - Al_p$) yields an approximation of allophane and imogolite (Parfitt and Childs, 1988). Sodium dithionite extracts of Fe_d represent the sum total of secondary Fe – namely, hematite + goethite + ferrihydrite – and for Al_d, a partial extract of secondary crystalline Al. Concentrations of Al_d continue to be reported although their importance in stratigraphic work is uncertain and these extract values should be used with caution (Birkeland et al., 1989).

Given the uncertainty and adjustments that have been made with the use of Fe and Al extracts, the work of Parfitt and Childs (1988) established a firm footing for several extracts of both elements. Whereas, Fe_p is of uncertain use, Fe_o and Fe_d concentrations yield approximate values for ferrihydrite (secondary hydroxide) and Fe_d, the sum total of extractable crystalline Fe, respectively. Because Fe_d has been known to measure concentrations of secondary Fe since the seminal work of Mehra and Jackson (1960), many workers have concentrated on using

* Corresponding author at: Department of Geography, York University, N. York, Ontario, Canada, M3J 1P3.
E-mail addresses: arkose@rogers.com (W.C. Mahaney), thamilton@camosun.bc.ca (T.S. Hamilton), barendregt@uleth.ca (R.W. Barendregt), ronhancock@ca.inter.net (R.G.V. Hancock), ppcosta@fc.ul.pt (P. Costa).

it to measure concentrations of secondary hematite, goethite and ferrihydrite in soils and paleosols. Despite the partial solubility of ferrihydrite, the ratio Fe_o/Fe_d is often used to approximate the build-up of ferrihydrite against ferrihydrite + goethite + hematite over time. Since Fe_o has an affinity for water-saturated conditions, corresponding increases of Fe_o in a section probably indicate phreatic conditions or a perched water table (Mahaney and Fahey, 1988) at some time in the past rather than reaction with magnetite. Given the variable but low concentrations of magnetite reported here, the Fe_o trends should be treated with caution as values may likely be overestimates of Fe_o in some horizons. However, to test the possibility of Fe_o reacting with magnetite we ranked Fe_o against Fe_t (Fe_o/Fe_t) in three sections having a magnetite increase downward to determine if Fe_o increased with depth. Despite a gradual increase of magnetite with depth, the ratio Fe_o/Fe_t does not show corresponding or anomalous behavior.

When coupled with total Fe (Fe_t) it is possible to calculate the relative age of soil formation using the function Fe_d/Fe_t (Mahaney et al., 1999, 2010) which measures the slow release of goethite + hematite + ferrihydrite with time. Similarly the arithmetic function $Fe_d - Fe_o$, normally used to calculate the approximate concentration of goethite plus hematite minus ferrihydrite, can be used with certainty in this instance. Lattice Fe ($Fe_t - Fe_d$), which diminishes with age, should be inversely related over time barring redox fluctuations caused by a drop in the water table.

Within the Al extract group, the concentration Al_p acts as a proxy for organic carbon and the ratio Al_p/Al_t may be used to test movement within a section or profile. Thus, increases in Al_p down-profile are approximated with translocation of organic carbon, which remains one of the principal tests of a spodic horizon in Spodosols (Podzols) (Soil Classification Working Group, 1998; NRCS, 2004).

Extracts of Fe and Al are used here, along with other mineral and chemical data, as age and paleoenvironmental indicators for the weathering of sediments in the oldest Early Quaternary moraine complex on Mount Kenya (Fig. 1a location; Fig. 1b topography). These residual chemical parameters also establish relative weathering indices between buried and relict paleosols and test organically-complexed Al as a proxy indicator of movement of organic carbon from surface epipedons for both relict (exposed) and buried profiles into subsurface horizons. Since the arithmetic function $Al_o - Al_p$ is considered a proxy for total allophane and imogolite (Parfitt and Childs, 1988), these two common poorly crystalline clay mineral concentrations were monitored down section at the three sites. Because both allophane and imogolite have been shown to undergo high rates of release in tephra-rich sediment (Hiradate et al., 2010), the trend of these common aluminosilicate weathering products from the top (low tephra) to bottom (higher tephra) in the three sections analyzed here, was established to test inferred allophane/imogolite distributions.

Furthermore, given the local stratigraphy and chronology established by Mahaney et al. (2013a), a test of climate and time factors on weathering and their influence on soil/paleosol morphogenesis is attempted.

2. Regional geology

Mount Kenya, part of the Central Plateau of East Africa, is a volcanic center with an intense and complex tectonic history since its inception during the Early Miocene (Baker, 1967; Schluter, 1997). The Eastern Rift valley of Neogene age follows an older Cretaceous rift lineament, with lavas issuing from fractures producing major mountains such as the Aberdares and Mount Kenya with the summit for the latter just over 5100 m asl.

The Mount Kenya massif is a volcanic succession with a thickness of ~6200 m overlying the African basement series (Baker, 1967; Vernacombe, 1983; Ries et al., 1992). Outpourings of Late Miocene to Pliocene mafic volcanics, sourced from the mantle (Rogers, 2006; Dawson, 2008), were accompanied by eruption of tuffs and agglomerate

in the early phase of mountain building. The mountain entered a major constructive phase by mid-Pliocene time, undergoing a final eruption of the main vent at ~2.71 Ma (Veldkamp et al., 2007), the later event coinciding with net updoming of the Eastern Rift Valley. Mount Kenya must have been close to its present elevation or higher to allow glaciation to start by ~2.0 Ma or before (Mahaney, 1990). Estimates of erosion of the summit area of the mountain vary from >2000 m (Gregory, 1921) to <1000 m (Mahaney, 1990) but the present valley floors were well incised by the time of the Olduvai Event (~2 Ma). The mountain has been stable since Late Pliocene time with minor faulting showing offsets of only tens of meters (Mahaney et al., 2011).

The history of glaciation on Mt. Kenya is extensive. The oldest glaciations named, from oldest to youngest, Pre-Gorges, Gorges and Lake Ellis [Fig. 2 (Mahaney, 1990; Mahaney et al., 2013a)], are known only from moraines on the eastern (Gorges Valley, Fig. 1a, b) and southeastern flanks of the mountain and are important in the context of this study because they represent the early stage of glacial growth on one of the highest tropical mountains on Earth. Herein, normally magnetized glacigenic sediments and bedrock with reversed overprints are, in turn, overlain with either reversed or normal beds/horizons considered to represent the Olduvai subchron with Late Matuyama overprints. The inherent test here involves a correlation of paleomagnetic data (Mahaney et al., 2013a) against characteristics of the paleosol profile and chemical signatures of Fe/Al extracts as indices of weathering and translocation.

Is the long punctuated weathering history of these multistory pedostratigraphic complexes coeval with the paleomagnetic chronology? Are loess-stripping/deflation episodes (Barendregt and Mahaney, 1988; Mahaney et al., 1997) as described in other similar-age profiles from this region recognizable in this paleosol sequence or are they different? These are some of the questions that prompted the analyses described below.

3. Materials and methods

On Mt. Kenya, sample pits were excavated and cleaned back to expose fresh sediment in the oldest terminal moraine system in Gorges Valley (Fig. 1). Of the 26 sections of Gorges-age moraine examined on the eastern flank of the mountain, three (GOR64, 68, 69) were selected in lower Gorges Valley for detailed pedological, petrographical and chemical analyses, as reported here. The soil descriptions used are genetic and follow guidelines set out by the NRCS (2004, and Soil Survey Staff, 2010). Some exceptions in horizon nomenclature apply here insofar as horizon designations follow the Canadian system (i.e. Ah for humus rich A horizons), Cox for oxide-rich C horizons (Birkeland, 1999). The 'ox' designation implies a yellow-reddish color stronger than 10YR 5 or so. The designation 'm' refers to cemented material (Schoeneberger et al., 2002; Soil Survey Staff, 2010). Soil color assessments follow the color chip system of Oyama and Takehara (1970). At least 500 g samples were collected from each horizon in each section to allow for particle size, clay mineral, and geochemical analysis of total Fe and Al. Particle size analysis followed procedures outlined by Day (1965). Samples were wet sieved to separate sands from clay plus silt, the sands subsequently dried and weighed out to the nearest hundredth of a gram. The silt/sand boundary of 63 μm follows the Wentworth scale; the silt/clay division used is 2 μm (NRCS, 2004).

Organic carbon was determined by loss on ignition (LOI) at 400 °C after 15 h following procedures outlined by USDA (NRCS, 2004); while total N was measured by Leco CHN Autoanalyzer. Total C and CEC were cross-checked with organic C to ensure no carbonate was present. Cation exchange capacity (CEC) was determined by the ammonium acetate method of Peech et al. (1947) and Schollenberger and Simon (1945). The pH of the <2 mm fraction was determined by electrode on a 1:5 solution (10 g mass:50 ml distilled H_2O) and the concentration of total salts by conductivity (Bower and Wilcox, 1965).
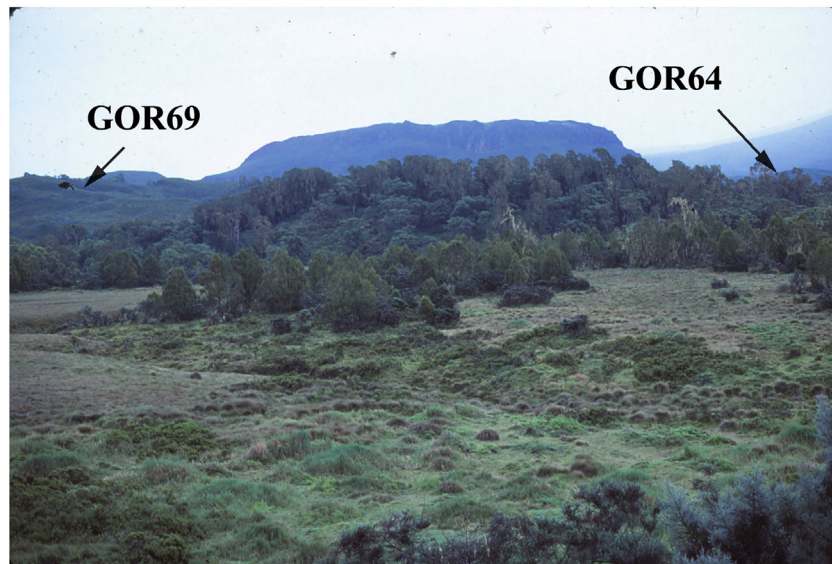
a
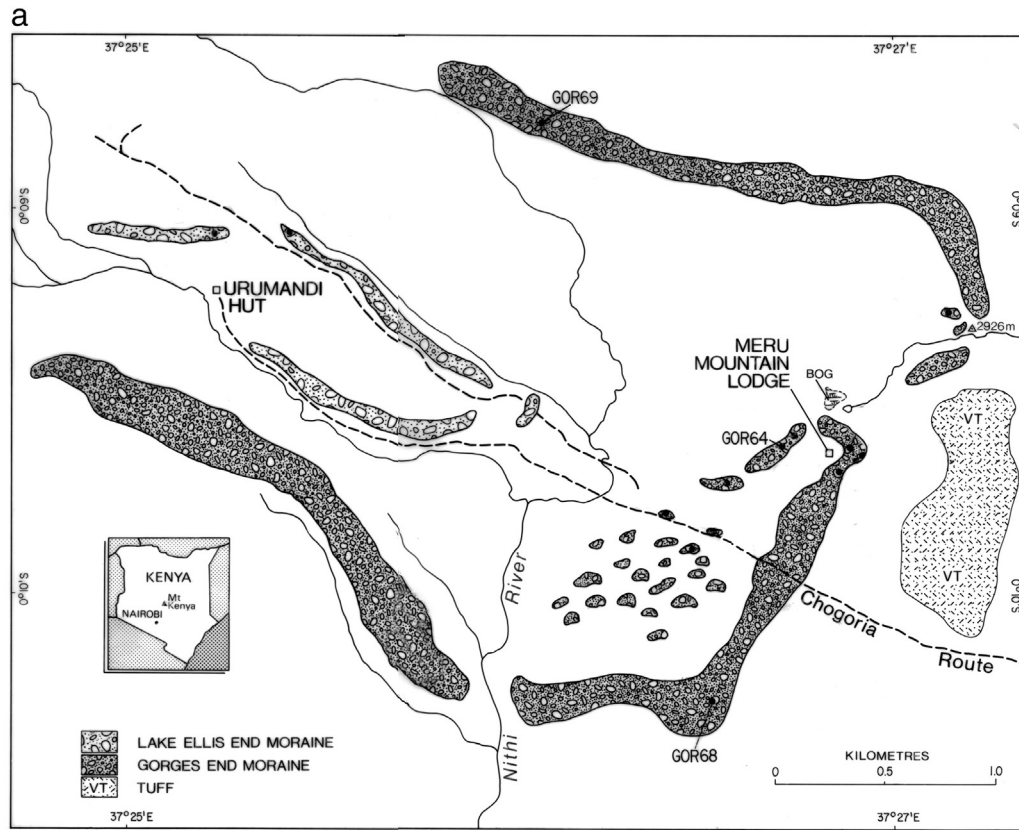
b

Fig. 1. a, Location and position of sites on the Gorges moraine complex, east flank of Mt. Kenya; b, Photo of the Gorges terminal moraine showing scattered forest of *Podocarpus* and *Hagenia* species 50 m above the nominal timberline. Mounds (center) on ground moraine of Gorges age are the result of mole activity (bioturbated) or remnants of deflation caused by katabatic and anabatic winds.

The Fe_d and Al_d extractions were made from 1 g (<2 mm fraction) subsamples, with sodium dithionite, as well as Na-citrate buffers releasing crystalline, amorphous, and organically-bound forms of Fe and Al, following criteria set out by Coffin (1963). Processed in the dark, to avoid photo-oxidation, acid ammonium oxalate was used to extract ferrihydrite (Parfitt and Childs, 1988) following McKeague and Day (1966). Subsequently, concentrations of Fe and Al were determined by atomic absorption spectrophotometry (AAS) using a Perkin Elmer 373 instrument, calibrated with appropriate bracketing standards. Instrumental neutron activation analysis (INAA) followed methods identified by Hancock (1984) to measure total Fe and Al in the <2 mm fraction of the soil samples. XRD analysis of the <2 μm fraction using oriented mounts followed methods outlined by Whittig (1965).

Sediments were sampled for paleomagnetic analysis by pressing plastic cylinders (2.5 cm diameter) into clean vertical faces. Remanent magnetization was measured using a JR-5A spinner magnetometer (Agico, Brno). Stepwise alternating field demagnetization (10–100 mT) proved sufficient to magnetically cleanse the specimens. Viscous normal
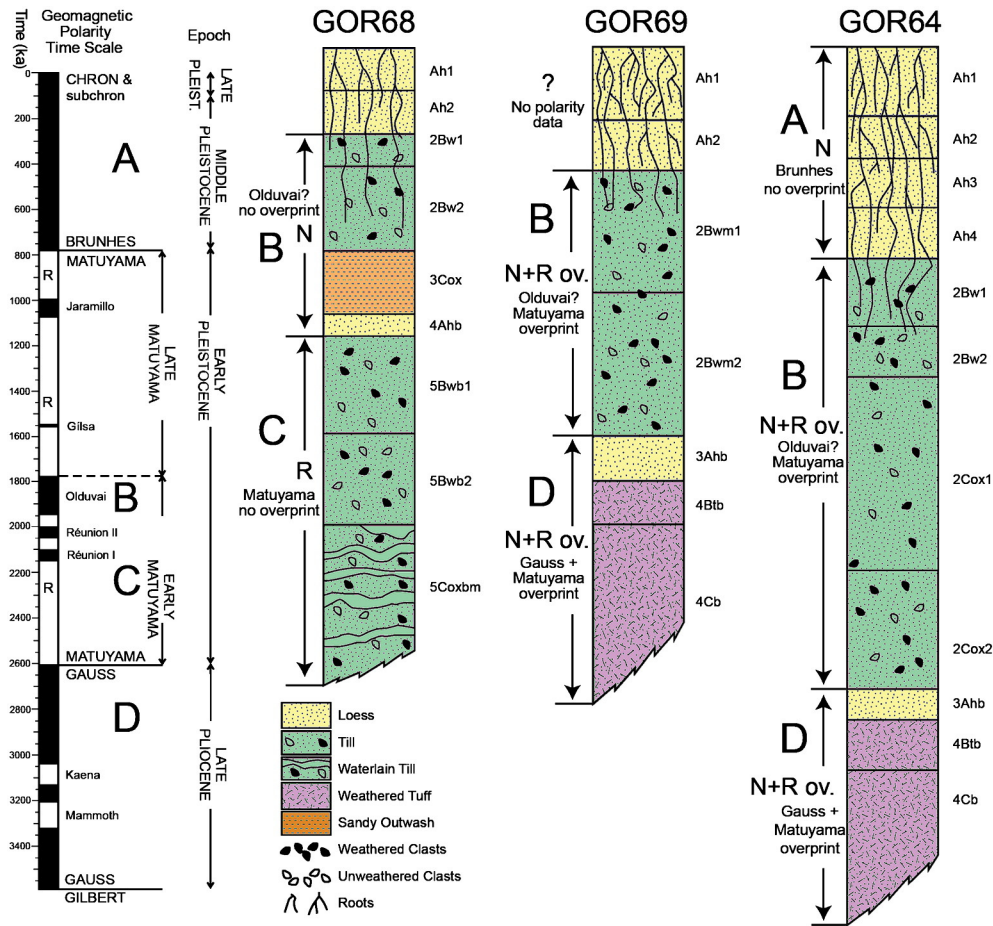
Fig. 2. Stratigraphy and paleomagnetic ages assigned to GOR64, 68 and 69. Magnetostratigraphy of three representative Gorges Valley sediment sites, Mt. Kenya comprises: Unit D, normally magnetized weathered bedrock with reversed overprint, of probable late Gauss age; Unit C, reversely magnetized till without overprints, of probable Early Matuyama age; Unit B, normally magnetized till and outwash, some samples exhibiting reversed overprints, of probable Olduvai age; and Unit A, normally magnetized sediments without overprints, of probably Brunhes age. Gorges age tills are in unit B, pre-Gorges till in unit C.

overprints were removed by 20 mT demagnetization, following methods outlined in Nelson et al. (2009) and Duk-Rodkin et al. (2010).

Data were compiled in Excel spreadsheets that were later exported to Statistica 10.0 for more detailed and precise statistical analyses. After this stage, charts were plotted and correlations attempted.

4. Results

4.1. Stratigraphy

The three pedostratigraphic sections (Fig. 2) consist of two profiles each: one at the surface representing sediment exposed for variable lengths of time following cessation of the Gorges Glaciation at some unspecified time but presumably during or just after the Olduvai Event (ca. 1.8 Ma); the second, a buried suite of paleosols in weathered bedrock or till pre-date the Olduvai Event, the latter referred to as the pre-Gorges Glaciation (Mahaney et al., 2013a). Till thicknesses vary from just over a meter to less than 0.5 m and presumably represent a minimum for the original deposits. Truncated boundaries between surface and buried paleosols are considered to represent erosion during glacial oscillations. At one of the sections [(GOR68) (Fig. 2)], a glacial outwash (3Cox horizon) is present, whereas in others it is missing. The magnetostratigraphy of these sections is described in Mahaney et al. (2013a) and the history of glaciations and magnetostratigraphy of glacial/interglacial sediments and paleosols on Mt. Kenya are outlined in Barendregt and Mahaney (1988), Mahaney (1990) and Mahaney et al., 1997).

Within the lower buried profiles, paleomagnetic analysis (Fig. 2) depicts either older Ahb horizons, some with reversed overprints (GOR64 and 69), or one (GOR68) which is normally magnetized and probably dates to the Olduvai subchron of the Matuyama Reversed Chron (~ 1.8 Ma). The lack of a reversed overprint in the surface profile of GOR68 is difficult to explain given the weathered grains resident there but may be related to pervasive deflation or to lower initial Fe content. Despite the lack of an s-shaped curve in particle size curves for the Ahb horizons, their silty compositions (Fig. 3a–c) and lack of pebbles are taken to indicate a largely aeolian origin. Below these uniformly thin Ahb horizons, subsurface horizons are either composed of weathered bedrock (GOR64, GOR69) or weathered till (GOR68), the latter possibly a signature of a pre-Olduvai (Pre-Gorges) glaciation. The lowermost horizon in GOR68 reveals stratification indicating a waterlain till (Fig. 2). Given the fact that paleomagnetic measurements can be readily obtained from these sediments (Barendregt and Mahaney, 1988; Mahaney, 1990; Mahaney et al., 2013a), till deposition must have been of a less viscous nature, perhaps not that of a liquid slurry as evidenced by the sediment character of the 5Coxbm horizon, but certainly with a sufficient water content allowing magnetic grains to become oriented in the earth's ambient field at the time of deposition. Of primal importance is the presence of Bt horizons in both GOR64 and GOR69, which signals downward translocation of clay during pedogenesis, a process that could only occur with the presence of continuous forest implying a higher timberline and a more humid microclimate than today. The horizons are thin but nevertheless heavy with clay, quite in contrast to GOR68, which carries a buried B horizon complex

complete with etched and corroded grains but without any evidence of clay movement.

The relative ages of loesses, paleosols, and tills described here were established by paleomagnetic analysis and are shown to range from the early Matuyama (2.6 Ma) for the initial stages of weathering, to the mid-Matuyama for the initiation of major glaciations on the mountain. The Gorges glaciations and associated interglacial deposits range in age from the mid-Matuyama to the early Brunhes Chron (~0.78 Ma). These relative ages can be further tested by examining variations in concentrations of Fe_d/Fe_t, as well as other mineral and chemical trends.

4.2. Profile morphology

The three sections reveal similar stacks of profiles, the surface paleosols consisting of admixtures of aeolian-influxed sediment marked by Ah horizons forming surface pedon epipedons. Below, the B and C horizons are comprised either of till (GOR64 and GOR69), or till and/or outwash (GOR68). Grouped together, the surface profiles represent the bulk of sediment weathered over a period of <2.0 Ma. Below, in the buried units, similar successions of 3Ahb (GOR64 and GOR69) and 4Ahb (GOR68) horizons consist of loess overlying buried B and C

horizons of weathered till (GOR68) or weathered bedrock (GOR64 and GOR69). The loessic input in the Ahb horizons is either apparent from higher silt content (GOR64; Fig. 3a, GOR68; Fig. 3b) or from translocation of silt downward into B and C horizons (GOR69).

Surface epipedons (Ah horizons) show considerable complexity with various horizon splits. The particle size analysis (Fig. 3a, GOR64; Fig. 3b, GOR68; Fig. 3c, GOR69) of these horizons shows considerable clay content (4–38% but generally 15–38%) with high organic carbon content of ~10–12% (detailed in the chemistry subsection below), much of which is inert to attack by 10% HCl, and is presumably lignin rich (Mahaney et al., 2013a). Mean phi calculations of particle size distribution curves (Fig. 3a–c) show various shifts depicting clay movement of different magnitude, sometimes within the Ah horizon group (GOR64; Fig. 3a) and always in the Btb horizons of GOR64 and 69. Otherwise mean particle size centers between 5 and 7 phi (with occasional variations of 1–9 phi) depending on weathering intensity. Soil structures are granular in the Ah horizons but below that any original structure has been destroyed by compaction over a long time interval. The high clay content insures variations of firm moist consistence within this group of samples along with near to full plasticity and slight to very sticky properties. The B horizon group carries the subscript 'w' to suggest
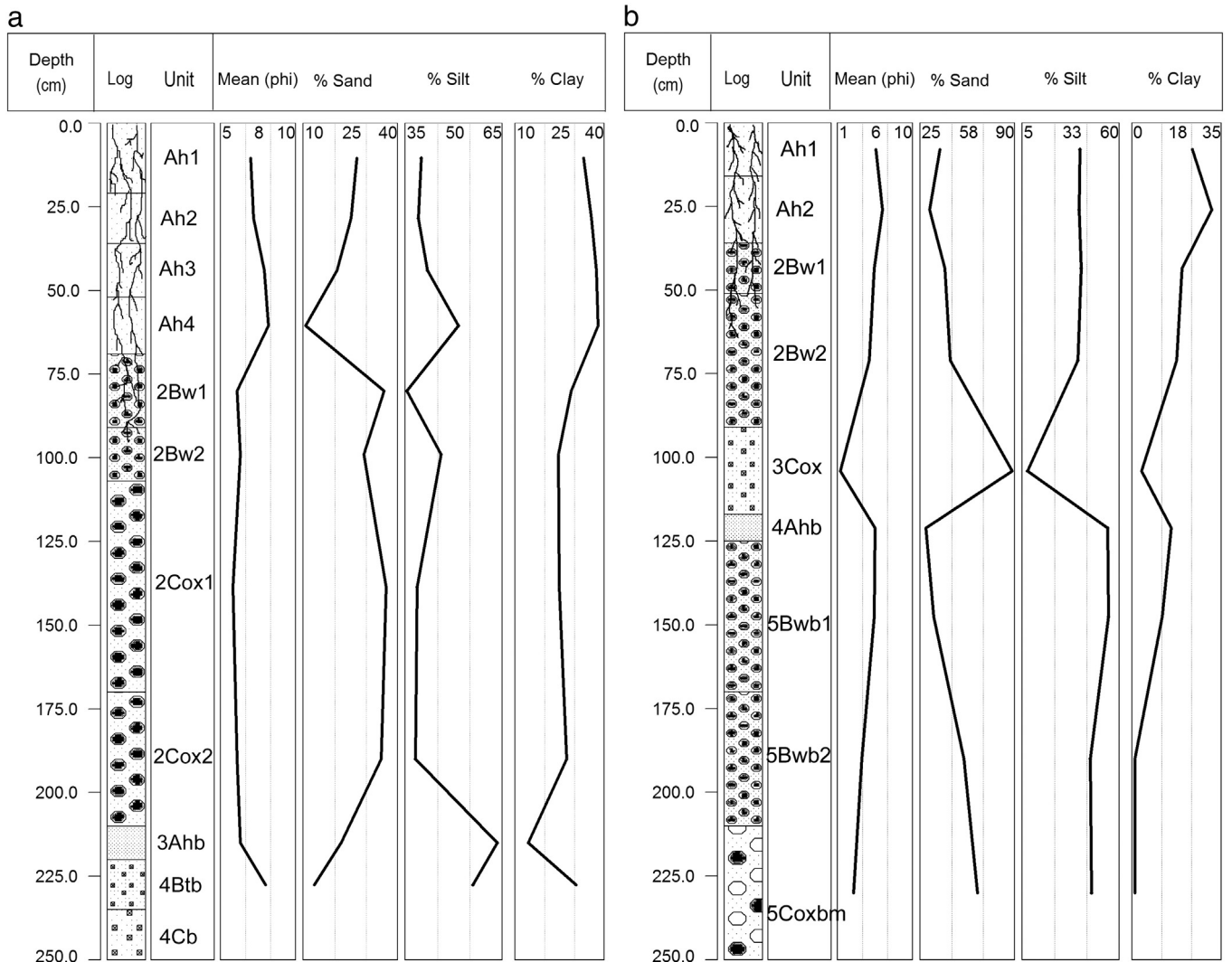
Fig. 3. Particle size distributions and mean particle size calculations: a, GOR64; b, GOR68; and c, GOR69. Particle size distributions down-profile in each paleosol provide a measure of clay production per the lower vs. the upper paleosol groups. Trends indicate degrees of aeolian contributions in the Ahb horizon group compared with surface epipedons. Mean particle size calculations and trends in each profile are useful for gauging degrees of clay production and translocation.

C
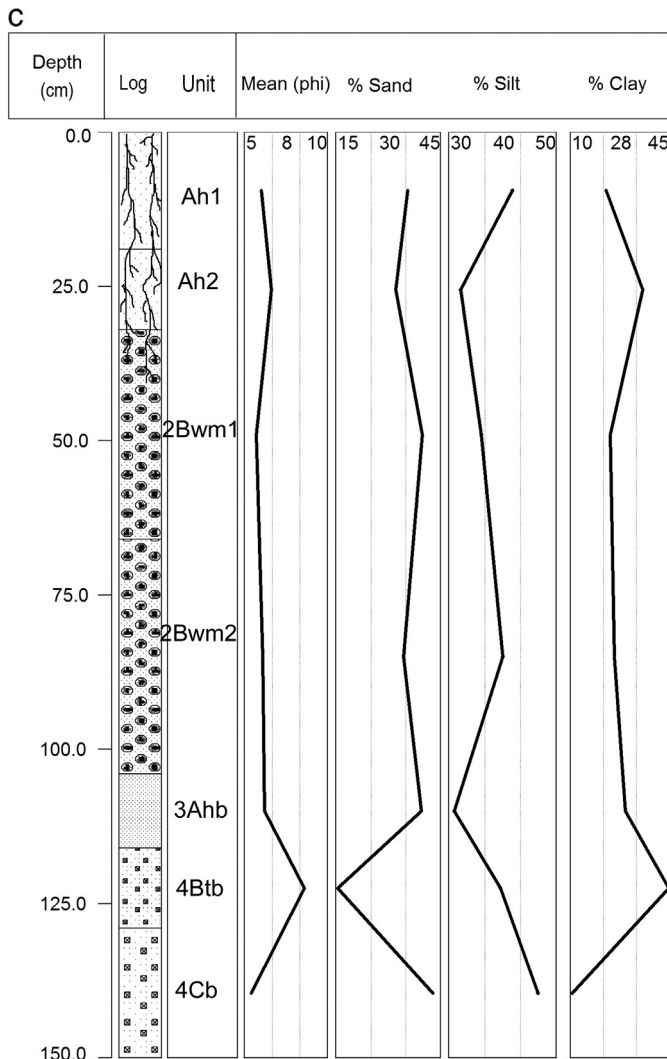
Fig. 3 (continued).

weathered conditions, or 't' (ton in German = clay) to represent clay influx (NRCS, 2004) and usually overlies a Cox horizon of either till or outwash.

Horizon thickness is subject to some uncertainty given that the buried paleosols have been overrun with ice and subjected to compression of overburden deposited later in their evolutionary history. Along with this, deflation (Mahaney et al., 1997) may have affected the buried pedons leaving only residual weathered material behind, which may explain the extreme variability of particle size distributions that range from 1–45% (Fig. 3a–c). Because the surface profiles have similar well-weathered minerals in place, it is likely they either escaped extreme deflation processes, or that incoming sediment replacement consisted of well-weathered material from up-slope. Certainly the Ahb horizons represent a minimum thickness of weathered sediment which was originally considerably thicker.

4.3. Sand petrography

Analysis of the sand fraction by petrographic microscope revealed traces to a few percent of organic matter, partially mineralized in some instances with cellulose and lignin, tough protein-sheathed seeds and charcoal. Considerable variability exists in the magnetic strength and preservation of magnetite in these samples, the dominant source material being aphanitic volcanic rock fragments (VRFs) and tephra. In addition to VRFs, volcanic phenocrysts are common with lesser plutonic

and metamorphic rock fragments, the latter presumably from the underlying African basement complex. Most of this material might be reduced in size and weathered but is not pervasively altered to clays and residual oxides, at least insofar as clay/oxide coatings exist in the sand fractions. These fractions are fine enough to have been derived from xenoliths which are common in mafic to intermediate tephras. Many grains exhibit variability in their preservation from fresh to weathered, which is the hallmark of reworked weathered sediment mixed with fresh aeolian delivered allochthonous grains and grains with weathered armored surfaces. Calcite is rare and microscopically detected by the occasional faint acid reaction which follows from the chemical analysis carried out on the bulk sample (<2 mm fraction; Table 2A). Clay balls and limonite concretions readily disaggregate or gelatinize and bleed/leach in acid.

The degree of preservation of organic matter is exceptional, especially in the Ahb horizons where recovered specimens are not readily hydrated and show no reaction to HCl. Recognizable fragments of stems, twigs, needles and bark appear as lignin-rich entities very resistant to chemical attack. Some samples might be reworked (down-worked) surficial materials, previously dried out and resistant to microbial degradation or they may have formed in place from long-term weathering in situ.

Within the surface profiles of the three sections, the soil epipedons (Ah group of horizons) are dominated with polycrystalline aphanitic VRFs comprising variable mixes of plagioclase in groundmasses of dark glass with traces of pyroxene and magnetite. Many grains appear as residual phenocrysts weathered away from more reactive glass or finer grained materials. The sands carry 5 to 10% residual, dark carbonized plant matter, an amount similar to what is reported below in the chemical analysis of the bulk fraction. Only a small percentage of detrital grains and VRFs are attracted to a magnet. Aside from somewhat higher Fe-oxide patinas on grains in GOR69, the samples contain a higher proportion of magnetic grains. The sands in the GOR68-Ah group are more highly weathered grains with a greater percentage of clay coatings and detrital quartz is more common along with black woody charcoal.

Analysis of the B/C group of horizons in the upper paleosols reveals variable percentages of magnetic grains and black VRF particles, the majority comprising residual feldspar and quartz. The magnetic fraction includes yellow coated grains with iron oxyhydroxides and traces of carbonized plant matter. In some cases (GOR69) etched sand grains are more common and in the lower Cb horizon grains are more highly etched and corroded. In GOR68, VRF grains are more vesicular than in the other two profiles with linings of clay and opaline silica. Some quartz grains are rounded, partially coated with black Fe/Mn oxyhydroxide rinds but because they are common only to quartz they may represent an admixed pre-weathered component. Rinds on sands carry fine laminae archival records similar to more robust weathering rinds on surface clasts, many of the latter carrying complex biomineralization (Mahaney et al., 2013b).

The buried Ahb epipedons are a class unto themselves in that they contain abundant dark olive brown sands (GOR64) with many organic coated VRFs and abundant tuff and tephra particles. Because of the dull surface luster of many grains this sample appears more highly weathered compared with the Ah horizon above. GOR64 also contains a high percentage of magnetic grains with less reaction to acid. In contrast the GOR69-3Ahb presents a more vigorous reaction, an observation supported by the Fe_o concentration reported in Table 3 below. However the degree of release of oxyhydroxides appears similar to GOR64-3Ahb. The GOR68-4Ahb is different again, being comprised largely of volcanic tephra with reddish particles that may have been oxidized largely in air as microscoria prior to deposition. Rare single crystals of quartz may be related to aeolian influx. Armored organic particles show a faint reaction to acid.

Within the buried B/C horizons, weathered brown to light orange colored sands clustered about the 500 μm grade size (GOR68) are highly oxidized, with glass showing appreciable coatings of orange Fe-oxihydroxides. Quartz is rare and black charcoal comprises less than

5% of the material. The lower Bwb horizon (5Bwb2) in GOR68 is less weathered and shows an affinity with the Ahb horizon above which suggests the wetting depth may extend to contact with the underlying 5Coxbm horizon. Similar coated grains, as in the upper 5Bwb1 horizon in GOR68, appear in GOR64, with a high percentage of magnetic grains with a faint reaction of acid implying carbonized organic fragments.

4.4. Clay mineralogy

The mineralogy of the <2 μm fraction (Table 1) was analyzed to determine the concentration and distribution of clay and primary minerals as well as alteration products. Halloysite minerals, principally metahalloysite, exist in both trace to small quantities in GOR64 and 69 while GOR68 is completely bereft of this species. A parallel to this is the distribution of gibbsite which exists as discontinuous quantities of trace strength in GOR64 and 69, rising in the lower profile of GOR68 to small amounts. This relationship may result from aggressive leaching which could strip Si from clay minerals leaving Al-hydroxide behind as seen in other Mt. Kenya chronosequences (Mahaney, 1990). Quartz ranges from trace to moderate quantities with somewhat higher amounts in the Ah group of horizons, the possible product of aeolian influx (Mahaney, 1990). Pyroxene and plagioclase minerals exhibit a staggered trend down section, somewhat higher concentrations with plagioclase increasing in the lower horizons. The amount of goethite is higher compared with hematite in (GOR64), and vice versa in (GOR69), which might imply that GOR 64 is younger given the tendency for goethite to weather to hematite. With goethite and hematite, both minerals are more abundant in the lower profile of GOR68, a possible reflection of either longer time for weathering, increased diagenesis and/or stronger climate (higher temperature/increased humidity) in the initial Late Pliocene/Early Pleistocene weathering episode.

Table 1
Mineralogy[a] of the clay fraction of the GOR paleosol succession.

Horizon	H	I	Q	Gi	He	Go	Pyx	Mt	Pl
GOR64									
Ah1	x	–	xx	tr	tr	–	tr	tr	x
Ah2	x	–	x	tr	tr	tr	tr	tr	x
Ah3	–	–	–	tr	tr	tr	x	tr	tr
Ah4	–	tr	x	tr	tr	x	x	–	x
2Bw1	x	–	tr	tr	tr	x	tr	–	x
2Bw2	x	tr	tr	tr	tr	x	tr	tr	x
2Cox1	tr	–	tr	x	tr	x	tr	–	x
2Cox2	tr	tr	tr	tr	–	–	–	–	x
3Ahb	–	–	x	tr	tr	–	tr	–	tr
4Btb	–	–	x	x	tr	tr	tr	–	tr
4Cb	–	–	x	x	tr	tr	tr	–	tr
GOR68									
Ah1	–	–	xx	–	tr	tr	x	tr	x
Ah2	–	–	xx	–	–	tr	tr	–	x
2Bwm1	–	tr	x	–	–	tr	x	tr	x
2Bwm2	–	tr	x	–	–	–	tr	–	tr
3Cox	–	tr	xx	–	–	–	x	tr	x
4Ahb	–	–	x	–	x	tr	x	tr	x
5Bwb1	–	–	xx	tr	x	x	–	tr	x
5Bwb2	–	–	xx	tr	x	x	–	tr	x
6Coxbm	–	–	x	–	tr	tr	x	tr	xx
GOR69									
Ah1	tr	–	x	tr	x	–	x	–	x
Ah2	tr	–	x	tr	x	tr	tr	tr	x
2Bwm1	x	–	–	tr	tr	tr	–	–	tr
2Bwm2	x	–	x	x	x	tr	tr	–	tr
3Ahb	–	tr	x	tr	tr	tr	tr	tr	tr
4Btb	–	–	x	tr	x	tr	x	–	x
4Cb	tr	–	tr	–	tr	x	–	tr	xxx

[a] Minerals are halloysite (H), illite (I), quartz (Q), gibbsite (Gi), hematite (He), goethite (Go), pyroxene (Pyx), magnetite (Mt) and plagioclase (Pl). Semi-quantitative mineral amounts are calculated as follows: – = nil, tr = trace, x = small amount, xx = medium and xxx = abundant.

4.5. Soil chemistry

The pH of the surface profiles (Table 2A) in the three sections shows some variation down-profile with profiles GOR64 and GOR68 showing strong acidity in the Ah group trending with minor overlap toward moderate acidity with depth to the contact with the buried Ah horizons. GOR69 grades from strong to moderate acidity with depth in the upper epipedon, thereafter with depth becoming strongly acidic. The buried profiles react somewhat differently with depth where the Ahb horizons range from very strongly acid to neutral becoming slightly to moderately acid (GOR64, GOR68) or very strongly to moderately acid (GOR69) with depth. In part, total salt data derived from conductivity analysis supports the pH with slight elevations where fresh organics at the surface are under decomposition, but for the most part, the electrical conductivity indicates a well-leached paleosol succession. Soil color, a common indicator of organic and Fe content, supports the different grades of acidity indicated by the range of pH and the well leached status of the profiles, both surface and buried. What is most apparent from the variation of hue is the stronger reddish color in the surface profile of GOR68 relative to GOR64 and GOR69, which is most probably a reflection of variable soil moisture or plant cover over time. The color intensity and chroma (Oyama and Takehara, 1970) indicate stronger organic inputs in GOR64 and GOR68 compared with GOR69, a trend correlating with organic carbon trends shown below in Table 2B. Color trends in the buried profiles show little relation to pH but hues darken with an increase of organic content.

The chemistry (Table 2B) of the three sections shows relatively high contents of organic carbon in the surface Ah horizons (range ~7–11%), which indicates the total percent organic matter in the soil matrix probably exceeds ~10–15% overall. Interestingly, organic carbon values are also high again in the Ahb horizons suggesting, either that carbon is translocated to depth in the surface profiles replenishing organic compounds in the buried Ahb horizons, or that the original carbon is long-lived, perhaps lignin-rich and extremely robust in the face of weathering energy as indicated in the petrographic analysis. Total C is

Table 2A
Selected physical characteristics, pH and total salts (EC) in the GOR succession, Mount Kenya.

Site	Horizon	Depth (cm)	pH (1:5)	EC[a] (mS/cm)	Color[b]
GOR64	Ah1	0–21	5.3	.33	7.5YR 2/1
	Ah2	21–36	5.3	.16	7.5YR 3/1
	Ah3	36–52	5.4	.12	7.5YR 3/2
	Ah4	52–69	5.5	.03	7.5YR 2/2
	2Bw1	69–91	5.5	.02	7.5YR 3/4
	2Bw2	91–107	6.0	.02	7.5YR 4/4
	2Cox1	107–170	6.1	.02	7.5YR 4/3
	2Cox2	170–210	7.2	.02	7.5YR 5/2
	3Ahb	210–220	6.3	.02	5YR 2/2
	4Btb	220–235	5.9	.03	7.5YR 4/4
	4Cb	235+			5GY 4/1
GOR68	Ah1	0–16	5.1	.13	5YR 2/2
	Ah2	16–36	5.5	.05	5YR 2/3
	2Bw1	36–51	5.8	.02	5YR 3/4
	2Bw2	51–91	5.9	.01	5YR 3/3
	3Cox	91–117	6.0	.01	7.5YR 5/6
	4Ahb	117–125	5.9	.02	5YR 2/1
	5Bwb1	125–170	5.8	.02	5YR 3/4
	5Bwb2	170–210	6.0	.02	2.5YR 2/3
	5Coxbm	210+	6.1	.02	5YR 5/6, 5/4
GOR69	Ah1	0–19	5.5	.17	7.5YR 2/2
	Ah2	19–32	5.8	.06	7.5YR 4/3
	2Bwm1	32–66	5.4	.08	7.5YR 4/4
	2Bwm2	66–104	5.2	.07	5YR 3.4, 4/4
	3Ahb	104–116	4.7	.15	5YR 2/3
	4Btb	116–129	4.9	.09	5YR 4/4
	4Cb	129+	5.6	.02	7.5YR 7/6

[a] Electrical conductivity.
[b] From Oyama and Takehara (1970).

Table 2B
Selected chemical properties of the profiles in the GOR succession.[a]

Site	Horizon	Depth (cm)	Total C (%)	Organic C (%)	Total N (%)	CEC (cmol/kg)
GOR64	Ah1	0–21	11.98	11.0	1.16	50.4
	Ah2	21–36	8.94	7.60	0.95	46.2
	Ah3	36–52	6.93	6.33	0.74	44.6
	Ah4	52–69	4.36	4.00	0.33	40.8
	2Bw1	69–91	1.00	0.76	0.13	21.4
	2Bw2	91–107	0.78	0.61	0.12	18.6
	2Cox1	107–170	0.44	0.38	0.06	14.4
	2Cox2	170–210	0.32	0.32	0.05	14.6
	3Ahb	210–220	5.06	4.23	0.52	70.9
	4Btb	220–235	1.58	1.48	0.15	28.6
	4Cb	235+	–	–	–	
GOR68	Ah1	0–16	7.81	7.36	0.78	37.8
	Ah2	16–36	4.60	5.12	0.45	31.2
	2Bw1	36–51	1.31	1.09	0.12	17.6
	2Bw2	51–91	0.63	0.58	0.10	11.0
	3Cox	91–117	0.09	0.06	0.08	7.2
	4Ahb	117–125	6.74	6.56	0.58	56.6
	5Bwb1	125–170	4.33	3.46	0.34	37.2
	5Bwb2	170–210	5.78	4.56	0.43	44.2
	5Coxbm	210+	0.14	0.18	0.09	22.6
GOR69	Ah1	0–19	8.18	8.24	0.75	45.4
	Ah2	19–32	4.27	3.74	0.43	33.4
	2Bwm1	32–66	1.25	1.22	0.15	22.8
	2Bwm2	66–104	0.71	0.66	0.13	18.0
	3Ahb	104–116	3.94	3.87	0.40	43.8
	4Btb	116–129	1.83	1.60	0.19	33.2
	4Cb	129+	0.11	0.20	0.04	32.8

[a] – = nil results.

Table 3
Iron and Al extract data for Sections GOR64, 68 and 69, Gorges Valley, Mount Kenya Afroalpine area. Data are in percent.

Horizon	Depth (cm)	Fe_p	Fe_o	Fe_d	Fe_t	Al_p	Al_o	Al_d	Al_t
GOR 64									
Ah1	0–21	0.66	0.95	1.80	3.94	0.94	0.97	0.48	8.1
Ah2	21–36	0.73	0.97	2.07	3.95	1.04	1.05	0.60	8.7
Ah3	36–52	0.85	0.94	1.94	3.95	1.28	1.21	0.71	9.7
Ah4	52–69	0.55	0.50	1.06	3.33	2.27	2.38	1.02	12.1
2Bw1	69–91	0.73	1.76	2.82	5.61	1.27	1.42	0.56	13.2
2Bw2	91–107	0.69	1.46	2.80	5.76	1.05	0.88	0.35	12.3
2Cox1	107–170	0.54	1.57	2.66	4.95	0.85	0.62	0.20	11.9
2Cox2	170–210	0.46	1.44	2.23	4.96	0.71	0.53	0.10	11.2
3Ahb	210–220	1.03	2.29	4.12	5.69	2.62	2.79	1.48	10.6
4Btb	220–235	0.97	2.70	4.39	7.01	1.71	1.83	0.81	12.7
GOR 68									
Ah1	0–16	0.99	1.91	2.91	3.06	1.33	1.53	1.11	8.3
Ah2	16–36	1.01	1.60	2.71	3.95	1.11	0.97	0.74	9.7
2Bw1	36–51	0.99	1.95	3.01	4.26	1.40	1.26	0.65	11.8
2Bw2	51–91	0.66	1.53	2.36	3.98	0.72	0.61	0.31	11.2
3Cox	91–117	0.15	0.88	2.35	2.54	0.23	0.33	0.11	9.0
4Ahb	117–25	1.68	2.47	4.20	5.02	3.08	2.78	1.85	9.1
5Bwb1	125–170	1.68	3.53	5.55	7.08	2.51	2.84	2.15	12.6
5Bwb2	170–210	1.59	3.06	5.50	6.73	3.36	4.08	2.70	10.2
5Coxbm	210+	0.29	2.25	4.50	6.22	1.18	3.42	1.60	11.6
GOR 69									
Ah1	0–19	0.75	1.61	2.43	4.63	0.54	0.84	0.64	9.1
Ah2	19–32	0.79	1.81	2.66	5.14	0.63	0.92	1.03	10.4
2Bwm1	32–66	0.49	1.30	2.72	6.65	0.49	0.71	0.56	11.3
2Bwm2	66–104	0.45	1.46	2.90	6.11	0.61	0.64	0.49	11.5
3Ahb	104–116	1.35	2.89	4.31	5.45	0.56	1.52	1.31	10.8
4Btb	116–129	1.09	2.37	3.73	6.91	1.43	1.37	1.05	12.2
4Cb	129+	0.08	2.10	4.29	8.41	0.11	1.17	0.86	11.7

sometimes up to 1% greater than organic C, possibly the result of carbonatite minerals, as otherwise it is not likely calcite could withstand the acidic pH of the soil microenvironment. Occasionally, it appears that minor instrument error or interference from other volatile elements may be to blame for organic carbon values in slight excess of total carbon. As expected, total N percent tends to follow organic carbon trends. The pH trends differ slightly among the three surface profiles, from strongly acidic in the surface horizons becoming moderately acidic with depth. In the older profiles below, the Ahb horizons show considerable variability from very strongly acidic in GOR69 and moderately acidic (GOR68) to slightly acidic (GOR64). The lowermost B and C horizons depict only slight pH variation in GOR64, values rising somewhat in GOR68 and 69.

The down-section CEC data (Table 2B) in each profile depict trends showing higher values in the surface epipedon group (Ah horizons) and in the Ahb horizons reflecting high organic carbon contents. Otherwise, in the surface profiles Bw/C horizons, lower CECs reflect the Si:Al (1:1) clay content of metahalloysite, values trending higher in the Bwb horizons in response to increased clay content. The standard test of removing the organic carbon influence on CEC (CEC/100 g clay; Birkeland, 1999) would simply reduce all values to <20 supporting the clay mineralogy discussed above. As a weathering index (Martini, 1970), the CEC/%clay ratio was not used in this case because of the high organic matter content (Bloesch, 2012) resident in both the surface and buried profiles.

4.6. Fe and Al extracts

The raw data for Fe and Al extracts are given in Table 3. The Fe_p distributions show relatively low concentrations down the surface profiles with slightly elevated levels in the Ah horizons, increasing into the buried profiles by ~150%. The exact composition of material in the Fe_p extract is unknown but XRD data on a number of samples establish that crystalline material is part of the load (Mahaney unpublished). The Fe_o distribution, without adjustment to ferrihydrite, yields lower levels in the surface profile epipedons increasing incrementally into the buried profiles. Because magnetite is thought to react with acid

ammonium oxalate (Walker, 1983), and petrographic analysis of the sand fraction indicates an increase of magnetite in the lower profiles of all three sections, part of the increase in Fe_o may result from laboratory preparation or from the flux of perched water over bedrock (GOR64, 69) and the one cemented Coxb horizon (GOR68). However, a portion of the increase in Fe_o with depth still suggests greater production of ferrihydrite in the lower profiles compared with the surface counterparts, even if the exact concentrations are in doubt. As expected from the Fe_o trend, Fe_d tends to follow a similar pattern although with higher concentrations, which supports the petrographic analysis. When Fe_d is compared with Fe_t (Table 4), the data unequivocally show that a large portion of total Fe has been converted to secondary Fe^{+3} forms and that this ratio narrows considerably with depth into the buried profiles. There are exceptions of course, as in GOR69, where secondary Fe is barely 50% of the total, but the high values overall and the difference between surface and subsurface profiles is rather a firm trend.

The Al extracts as discussed earlier are rather problematical with Al_o values sometimes exceeding Al_d concentrations. While the Al_o concentrations are considered to provide an approximation of imogolite and allophane once Al_p is subtracted, it is possible the Al_d values represent secondary forms of crystalline Al as previously suggested by Birkeland (1999) and Mahaney (1990), although with not all crystalline products fully extracted. The Al_p concentrations, taken alone and gauged downsection in all three sites, tend to correspond to nearly uniform distributions of organic carbon or increases of organic carbon in buried Ahb horizons. The real test of Alp translocations can only come from normalizing the values with Al_t and comparing the data with the organic carbon database in Table 2B.

The principal function of the Fe extract ratio Fe_d/Fe_t (Table 4) is to quantify the relative age of weathered sediment via the slow gradual increase of secondary Fe to total Fe. Correlating Fe_d values with the twin profiles in each section, it is obvious that age-quotients in the epipedons of the surface profiles have similar values to the understory

Table 4
Fe and Al extract functions for pedostratigraphic successions in the Gorges Moraine of Late Pliocene/Early Pleistocene age. Individual extracts are in percent calculated from data in Table 1.

Horizon	Depth (cm)	Fe_o/Fe_d	Fe_o/Fe_t	$Fe_t - Fe_d$	Fe_d/Fe_t	Al_p/Al_t	$Al_o - Al_p$
GOR64							
Ah1	0–21	0.53	0.24	2.14	0.46	0.12	0.03
Ah2	21–36	0.47	0.25	1.92	0.61	0.11	0.01
Ah3	36–52	0.48	0.24	2.01	0.49	0.13	Nil
Ah4	52–69	0.47	0.15	2.67	0.28	0.19	0.09
2Bw1	69–91	0.62	0.31	2.79	0.50	0.10	0.15
2Bw2	91–107	0.52	0.25	2.96	0.49	0.08	Nil
2Cox1	107–170	0.59	0.32	2.29	0.53	0.07	Nil
2Cox2	170–210	0.65	0.29	2.73	0.45	0.06	Nil
3Ahb	210–235	0.56	0.40	1.57	0.72	0.25	0.17
4Btb	220–235	0.62	0.39	2.62	0.63	0.13	0.12
GOR68							
Ah1	0–16	0.66	0.62	0.15	0.95	0.16	0.20
Ah2	16–36	0.59	0.41	1.24	0.69	0.11	Nil
2Bw1	36–51	0.65	0.46	1.25	0.71	0.12	Nil
2Bw2	51–91	0.65	0.38	1.62	0.59	0.06	Nil
3Cox	91–117	0.37	0.35	0.19	0.95	0.03	0.10
4Ahb	117–125	0.59	0.49	0.82	0.84	0.34	Nil
5Bwb1	125–170	0.64	0.50	0.53	0.91	0.20	0.33
5Bwb2	170–210	0.56	0.45	1.23	0.41	0.33	0.52
5Coxbm	210+	0.50	0.45	1.72	0.72	0.10	2.24
GOR69							
Ah1	0–19	0.66	0.35	2.20	0.52	0.06	0.30
Ah2	19–32	0.68	0.35	2.48	0.51	0.06	0.29
2Bwm1	32–66	0.48	0.20	3.93	0.41	0.04	0.22
2Bwm2	66–104	0.50	0.24	3.21	0.47	0.05	0.03
3Ahb	104–116	0.67	0.53	1.14	0.79	0.12	0.96
4Btb	116–129	0.64	0.34	3.18	0.54	0.12	Nil
4Cb	129+	0.50	0.25	4.12	0.51	0.01	1.06

Fig. 4. Box plot averaging out medians for three groups of horizons, ages determined partly from weathering criteria and partly from paleomagnetic data. Polynomial regressions of Fe_d/Fe_t/ages, the latter averaged for Gauss (2.6 Ma), Early Olduvai (2.0 Ma), and Late Olduvai (~1.8 Ma). Three groups of horizons in three paleosol sections show average Fe_d/Fe_t values of between 0.5 and 0.65, as indicated by a trend line, with one outlier (GOR68-Ah1) which must comprise greatly reworked Fe minerals. The wide standard deviation in the younger group of samples is probably partly due to organic dilution in the Ah horizons (less a factor in the older Ahb horizons due to hydrolysis) or to reworking of older weathered sediment.

horizons extending with depth to the Ahb horizons. There are variations where the quotient drops (GOR64) with depth in the Ah horizon complex, whereas in others (GOR68) it rises, or remains uniform (GOR69). Within the Bw group of horizons in the surface profiles, Fe_d while elevated, is seen to remain uniform (GOR64, GOR69), or increase with depth (GOR68), the latter signifying an increase in age. Within the buried profiles, Fe_d is either elevated (GOR64, GOR69) compared with the surface profiles, or remains relatively the same (GOR68). To some degree the increase in Fe_d is registered by stronger yellow–red colors (Table 2A) as in GOR64 and 69 while in other cases (GOR68) colors vary somewhat but remain essentially the same throughout.

Taking the paleomagnetic data (Fig. 2) for each of the horizons by groups (Gauss, Olduvai and < Olduvai/Upper Matuyama), as outlined by Mahaney et al. (2013a), and calculating the median value of Fe_d/Fe_t for each group (Fig. 4), produces a trend line depicting a slow rise from the surface profiles of 0.5 to buried units reaching 0.65. The difference of 0.15 in median quotients represents greater weathering energy during pre-Olduvai time. While the normal magnetization obtained from the surface epipedons (Ah group) of GOR64, and the complete surface profiles of GOR68 and 69 plus the lower 4Ahb horizon, might relate to the Olduvai and any of the younger normal events (Jaramillo, Brunhes), it is placed within the Upper Olduvai on the basis of weathering criteria outlined here. Despite the large range of Fe_d/Fe_t in the youngest normally magnetized (<Olduvai/Upper Matuyama) group, its close correlation to the median value of the Olduvai group indicates a similar median age, the large range likely a product of recycling of the mobile fine grain material in this highly charged aeolian Afroalpine environment. Interestingly, the range of Fe_d/Fe_t observations around the median values in the Olduvai and Gauss groups is significantly less, possibly the product of reduced aeolian activity which fits with the expected reduction of preglacial katabatic wind circulation and higher elevation of the timberline.
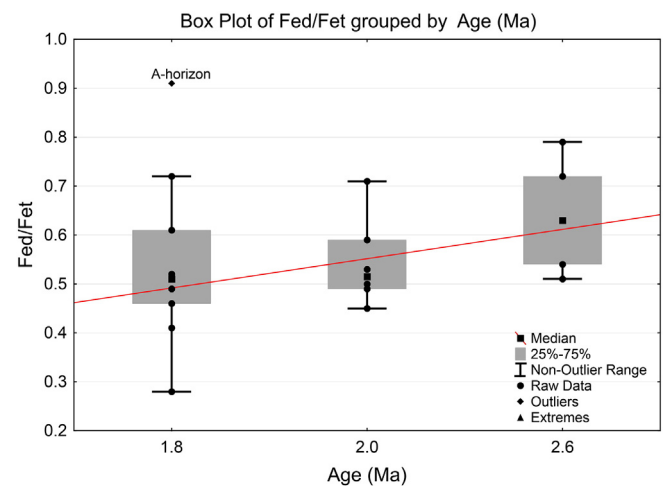
As a further test of age, the calculated concentration of ferrihydrite (Fe_o) (Table 4) shows a staggered increase in GOR64 — lower in the surface epipedon (Ah group), plateau increase of 150% to near 200% in the Bw/Cox group, leveling off in the buried profile (3Ahb/4Btb horizons). Again, a similar trend to GOR64 is evident in GOR69. The trend in GOR68 is different, since concentrations decline with depth in the surface profile, increase in the buried profile and decline again in the very bottom horizons. In all, the Fe_o, while slightly elevated from extract preparation, tends to follow the distributions of Fe_t observed in the petrographic analysis of the sand fractions. The distribution of Fe_o parallels that of Fe_d/Fe_t, corroborating two distinct populations of weathered sediment, a group with higher elevated indices comprising the lower profiles and a group with slightly lower indices which is not as weathered in the surface profiles.

A weathering index of the effect of climate and time on Fe release is inherent in the arithmetic relationship of $Fe_t - Fe_d$, the intent being to measure the amount of lattice Fe remaining in a sample. Since SEM/EDS (Mahaney et al., 2013a) and petrographic investigations of large populations of grains per horizon indicate a near uniform lithology within the upper profiles in each section with a 20–30% increase in Fe minerals with depth, the expectation is that at least in the upper profiles, lattice Fe should reflect leaching/weathering with depth. Overall, lattice Fe in the surface epipedons remains above 2% and is relatively constant in GOR64, GOR69, whereas in GOR68 it greatly declines in Ah1, leveling off in the lower epipedon. Within the Bw/Cox group of surface horizons there are minor variations again in GOR64 and GOR69 as lattice Fe increases relative to the overlying Ah group, which suggests the Ah horizons are not only acid makers but long-lived ones as well. GOR68 stands apart again with lower lattice Fe, presumably since it is more aggressively weathered and leached. Within the buried profiles, Fe_t is higher in GOR64 and 69 reflecting higher Fe in the bedrock compared with GOR68 which comprises a till with a mix of lithologies including additional quartz. Correspondingly, lattice Fe is higher in GOR64 and GOR69 and lower in GOR68 with the exception of the 5Coxbm horizon.

A measure of the translocation of Al, the ratio Al_p/Al_t shows nearly uniform distributions in the upper profiles with only very slight movement in the epipedon of GOR64. In the buried profiles slight increases in some Ahb horizons may reflect the relatively high organic carbon values (approximately 4–6% or about half the normal values in the Ah1

horizons of the surface paleosols). Movement of organic carbon is not registered in either of the two Btb horizons in GOR64 and GOR69 despite the movement of clay. The very low values of Al_p probably reflect microbial activity with a nearly steno soil temperature estimated to be about ~8 °C, nearly unvarying throughout the year (Mahaney, 1990).

Concentrations of Al_o vary somewhat erratically and tend to increase in the Ahb horizons. Similarly, crystalline Al given by $- Al_d -$ depicts an erratic trend with depth in the profiles. While Al_d was formerly considered to amount to secondary Al oxides (McKeague and Day, 1966) it often exhibits lower values than amorphous Al (Al_o). Because the Al_o values obtained here often exceed the crystalline Al (Al_d) concentrations, only the latter are used in soil classification studies (NRCS, 2004). As reported elsewhere (Parfitt and Childs, 1988; Birkeland et al., 1989; Mahaney, 1990; Mahaney et al., 1999) it appears that Na-dithionite fails to extract all secondary crystalline Al. However, Parfitt and Childs (1988) consider $Al_o - Al_p$ to approximate released allophane plus imogolite, two widespread but poorly crystalline aluminosilicate products. While calculations of this arithmetic function appear staggered through the sections (Table 4), depicting nil to 0.3% in the surface paleosol profiles, values increase markedly in the lower buried profiles from nil to 2.2%. The significance of the Al profile variation is that some horizons appear to have been more chemically active than others and also that the older buried profile in GOR64 may, in fact, be younger than GOR68 and GOR69, as suggested somewhat by the topographic displacement of moraine fronts shown in Fig. 1a.

5. Discussion

Unlike other paleosol sequences (Mahaney et al., 1999; Schülli-Maurer et al., 2007) where Fe_d/Fe_t increases with time in a chronosequence, the data presented here show two populations of paleosols in the GOR group: upper and lower, with the upper group containing reworked material from below and from other surrounding well weathered sites. In a two-dimensional sense, reworking of material from below into the upper profiles may be related to deflation prior to the ingress of glaciation, but in a three-dimensional sense, material could be transferred laterally within horizons and in tandem with groundwater fluxes. The increase of Fe_d in the lower horizons might be partly due to an increased content of Fe-bearing minerals, loss of Si from leaching and/or a more humid and warmer preglacial climate. This trend is paralleled by a sharp increase in Fe_o in the lower profiles, which is a product of additional ferrihydrite release and/or sample preparation. Spikes in the concentration of Fe_o with depth (Mahaney and Fahey, 1988) in any of the profiles may well signal strong reducing conditions with perched water at some time in the past and/or fluctuations in magnetite content of the parent materials. The Fe_o trends in all three sections are only interrupted with 'spikes' in the 5Bwb1 horizon of GOR68, possibly the 3Ahb horizon of GOR69 and the 4Btb horizon of GOR64, all known to have higher magnetite, thus confirming they could result from sample preparation. Otherwise the Fe_o trend with depth in all three profiles is one of slow decline with depth away from the acid producing Ah and Ahb horizons followed by an increase in the buried profiles. Clearly this is a situation where length of weathering time (surface pedons <2.0 Ma) comes close to equaling weathering in a buried suite of older paleosols (buried pedons) forming in a warmer and presumably wetter climate over a much shorter time frame (~0.5 Ma).

Variations in lattice Fe ($Fe_t - Fe_d$) may have involved reworking of old grains into younger epipedons (i.e. GOR68-Ah1), whereas in other profiles the surface epipedons are slightly lower in lattice Fe or about the same as compared with the subsurface horizons. The GOR69 profile shows a reduction of lattice Fe in the Ah1 followed by increases below in the upper profile, presumably a response to increased weathering in the surface or incorporation of pre-weathered materials by aeolian influx. Within the lower profiles, lattice Fe shows either a sharp reduction in the Ahb horizons (GOR64, GOR69) compared with the Btb horizons below or a slight reduction with a slow increase into the bottom of the

profile (i.e. GOR68). In all, considering the greater loss of lattice Fe in the lower group of paleosols, the data argue for well-weathered sediment with high ratios of Fe_d/Fe_t, the result of a long and variable weathering trend, first under a warmer and more humid preglacial climate followed by episodic weathering, faster under interglacial climates and slower under glacial ones. Even given increased Fe_t in the lower profiles, whether straight from bedrock (GOR64, GOR69) or mixed with glacial debris (GOR68), the early and largely pre-Olduvai weathering episode was shorter than the post-Olduvai Event but appears to have been influenced by a more aggressive paleoclimate in the former which supports previous microscopic and chemical (SEM/EDS) investigations of Mahaney et al. (2013a). The Fe data further suggest that some pre-weathered grains in the lower profile found their way into the upper profile either by glacial mixing or by aeolian transport.

The Al_p data strongly suggest little release of organically-bound Al which is curious because of the inordinately high Al_t throughout. High Al might result from Si leaching, and given the high rate of etching and corrosion (Mahaney et al., 2013a) seen throughout all three sections, it is likely Si removal has increased the concentration of Al_t. Little Al_p also might be attributed to microbial action over time.

Calculations of goethite/goethite + hematite made by Kämpf and Schwertmann (1983) in tropical soils showed that goethite is more responsive to moisture, organic carbon and low pH whereas higher temperature favors the formation of secondary hematite. Analysis of the raw data in the GOR sequence shows that Fe_d-Fe_o values increase with depth into the lower profiles in all three sections with some reworking of weathered products from the buried unit into the ground paleosol (upper unit). Presumably, these values are underestimations if one accepts the magnetite/oxalate overestimation of Fe_o, but the data do indicate an excess of hematite over goethite, a trend supported by the XRD analysis of the clay fraction (Table 1). While the 3000 m elevation on Mount Kenya is not inherently a kaolinite-forming climate, XRD analysis of the clay fraction in the GOR group clearly shows an excess of hematite over goethite (Table 1) in the lower profiles, a trend seen elsewhere (Kämpf and Schwertmann, 1983), all of which strongly suggest a stronger (warmer-wetter) climate during the morphogenesis of the buried paleosols.

Similarly, the ratio Fe_o/Fe_d, the 'activity ratio' of Dormaar and Lutwick (1983), formerly considered to measure the conversion of amorphous Fe (Fe_o) to crystalline forms (Fe_d), is now sometimes used to illustrate a reduction in Fe_o over time (Mahaney et al., 1999; Schülli-Maurer et al., 2007). This ratio is not readily applicable here given the variability of Fe_o and lack of trends with depth among all three sections. If there were truly a large scale influx of fresh materials to the surface epipedons in all three profiles, and if Fe_o/Fe_d is higher in younger sediment, this ratio should identify the aeolian input.

The wetting depth in paleosols, often marked by the depth of root penetration, here coincides with ~80 cm in GOR68, ~90 cm in GOR64 and ~50 cm in GOR69. While these depths may likely have changed during various glacial episodes, they appear to coincide closely with depletions in Al_p (Table 3). Because the paleosols are clay rich, it may be that wetting depths established in the first 100 kyr weathering episode become locked in place with little variation barring a large scale influx of soil water during one or more interglacials. To firm-up estimates of wetting depths from proxy Al_p trends one would need to work out field capacities and permanent wilting points of moisture in the profiles.

The presence of an older, buried till in the GOR68 section emphatically demonstrates that a glaciation preceded the Gorges event (Mahaney, 1990; Mahaney et al., 2013a). The question is when and how extensive was it? The presence of glacially-crushed grains in Early Quaternary lahars on the mountain (Mahaney, 1990) may well correlate with till in the lower profile of GOR68. The higher Fe_d values in the buried unit C, relative to the Gorges till within the surface profiles (unit B), argue for an older age for this lower till. Despite the attempt to

use Fe_o (Dahms et al., 2012), along with other oxihydroxides as a long-lived (~1 Ma) chronometer in the European Alps and the Rocky Mountains of N. America, we used only the Fe_d/Fe_t function, since Fe_o is partially soluble and subject to unknown rates of solution during interglacial periods and here it is compromised by the prevalence and persistence of primary magnetite.

To understand how and when glaciation began on Mount Kenya it is necessary to understand the exact timing of construction of the massif to an altitude that fostered retention of snow and development of glaciers. Assuming the mountain reached its maximum elevation at the time the plug rock crystallized at 2.71 Ma (Veldkamp et al., 2007), revised from 2.65 Ma (Everden and Curtis, 1965)], surfaces must have become stable soon thereafter allowing weathering to ensue in stable sites along with early glaciation. It is this earliest glaciation in the Early Pleistocene, or perhaps series of episodic ice advances, that is central to the discussion here. Late Pliocene/Early Pleistocene paleoclimate reconstructions using global benthic ^{18}O trends (Lisiecki and Raymo, 2005) invoke small amplitude climatic oscillations from cool/dry to warm/wet for much of East Africa, reverting after the Olduvai Event to cold/drier climate that probably led to early glaciation on the mountain. This trend is similar to the sequence of a dry climate deduced for the west flank of Mt. Kenya (Mahaney et al., 2011) during the Early Pliocene, reverting to a less dry climate toward the close of the epoch at the boundary with the Pleistocene. In this low elevation grassland environment the first ingress of loess from Pleistocene glaciation led to the development of argillic (Bt) horizons that may well have developed in conjunction with punctuated humid intervals prior to and across the Olduvai Event (Lisiecki and Raymo, 2005). It is these Bt horizons on the west flank of the mountain that probably correlate with similar weathering records (Btb horizons) in Gorges Valley (Mahaney et al., 2011). The Btb horizons in GOR64 and GOR69 probably formed during the high amplitude climatic intervals of 2.7–2.5 and 1.9–1.7 Ma interbedded with periods of aridification, as determined from detailed analysis of lacustrine records (Trauth et al., 2005).

Assuming the drier intervals in the Early Pleistocene correlate with glaciation, humid intervals with interglacial climates, it is likely that the earliest Pleistocene glaciations (pre-Gorges and Gorges) correlate with the first arid period of 2.5–1.9 Ma, the post-Gorges weathering with a drier interval (<1.7 Ma., Trauth et al., 2005). If this correlation is correct, then the Btb horizons in the GOR64 and GOR69 profiles had to form for the most part prior to 2.5 Ma, and the inference of expanded forest changing the microclimate at the site is on reasonably firm ground.

In summary, with some variability down profile in all three sections, the petrography shows a mix of weathered/fresh grains with a multitude of xenoliths and preweathered fragments that have likely been extensively reworked by aeolian and glacial processes, some many times over. Other grains appear to have lost armored surfaces, presenting fresh fragments that seem out of place in profiles that have been exposed to the subaerial atmosphere for variable lengths of time since the Gauss Normal Chron.

6. Conclusions

The build-up and distribution of Fe and Al extract concentrations over time present some unexpected twists to what are usually straightforward trends. The usual case on Mount Kenya is for fresh sediment superposed on older tills to yield lower Fe_d values, the result of deflation during times of severe downturn in climate with the advent of ice in the upper catchments. While this occurred in nearby areas (Mahaney, 1990; Mahaney et al., 1997) it does not seem to have affected the three sections described here. What is outstanding is the degree to which old grains are recycled from weathered bedrock and older till bodies into younger tills/outwash and aeolian sediment (surface epipedons) and later subjected to further weathering. While wetting depths are tentatively identified halfway into the surface profiles

there is little in the Fe release data to indicate much of a shift in weathering intensity over time.

While problems persist with the precise meaning of Al_o and Al_d over time, Al_p (raw data) shows some variation, partly responding to weathering depth and partly also to presumed microbial action, which with given soil temperatures of $+10\ °C$ at 3000 m is likely intense (viz: Mahaney, 1990). The Fe_d/Fe_t ratio as a geochronometer yields high ratios with some minor variations in the upper profiles of all three sections indicating a long weathering history, the product of episodic changes in climate from the Olduvai Event to the present. Increases in the ratio at depth in the older suite of paleosols may result partly from increased primary Fe-bearing minerals in the sediments and partly from a climate more ameliorative to weathering. Other Fe extract trends and arithmetic functions tend to support the Fe_d/Fe_t interpretations. Variations in Fe_o/Fe_d are probably related to partial dissolution of ferrihydrite, with possible reaction to differential ground water invasion and sample preparation.

Acknowledgments

References

Alexander, E.B., 1974. Extractable iron in relation to soil age on terraces along the Truckee River, Nevada. Soil Sci. Soc. Am. Proc. 38, 121–124.

Baker, B.H., 1967. Geology of the Mt. Kenya area. Geology Report 79.Kenya Geological Survey, Nairobi (78 pp.).

Barendregt, R.W., Mahaney, W.C., 1988. Paleomagnetism of selected Quaternary sediments on Mount Kenya, East Africa; a reconnaissance study. J. Afr. Earth Sci. 7, 219–225.

Birkeland, P.W., 1999. Soils and Gemorphology. Oxford University Press, Oxford, U.K.(430 pp.).

Birkeland, P.W., Burke, R.M., Benedict, J.B., 1989. Pedogenic gradients for Fe and Al accumulation and P depletion in arctic and alpine soils as a function of time and climate. Quatern. Res. 32, 193–204.

Bloesch, P.M., 2012. Prediction of the CEC to clay ratio using mid-infrared spectroscopy. Soil Res. 50 (1), 1–6. http://dx.doi.org/10.1071/SR11137.

Blume, H.P., Schwertmann, U., 1969. Genetic evaluation of profile distribution of aluminum, iron and manganese oxides. Soil Sci. Soc. Am. Proc. 33, 438–444.

Bower, C.A., Wilcox, L.V., 1965. Soluble salts. In: Black, C.A. (Ed.), Methods of soil analysis. American Society of Agronomy, Madison, Wisc., pp. 933–951.

Coffin, D.E., 1963. A method for the determination of free iron in soils and clays. Can. J. Soil Sci. 43, 7–17.

Dahms, D., Favilli, F., Krebs, R., Egli, M., 2012. Soil weathering and accumulation rates of oxalate-extractable phases derived from alpine chronosequences of up to 1 Ma in age. Geomorphology 151-152, 99–113.

Dawson, J.B., 2008. The Gregory Rift Valley and Neogene—Recent volcanoes of Northern Tanzania. Geological Society, London, Memoirs, 33 (102 pp.).

Day, P.E., 1965. Particle fractionation and particle size analysis. In: Black, C.A. (Ed.), Methods of Soil Analysis. American Society of Agronomy, Madison, Wisconsin, pp. 545–567.

Dormaar, J.F., Lutwick, L.E., 1983. Extractable Fe and Al as an indicator for buried soil horizons. Catena 10, 167–173.

Duk-Rodkin, A., Barendregt, R.W., White, J.M., 2010. An extensive Late Cenozoic terrestrial record of multiple glaciations in the Tintina Trench, west-central Yukon, Canada. Can. J. Earth Sci. 47 (7), 967–1002.

Everden, J.F., Curtis, G.H., 1965. The potassium-argon dating of late Cenozoic rocks in East Africa and Italy. Curr. Anthropol. 6, 343–385.

Gregory, J.W., 1921. The Rift Valleys and Geology of East Africa. Geological Society, London (479 pp.).

Hancock, R.G.V., 1984. On the source of clay used for Cologne Roman pottery. Archaeometry 26, 210–217.

Hiradate, S., Hirai, H., Hashimoto, H., 2010. Direct determination of allophane and imogolite in Andosols using nuclear magnetic resonance spectroscopy. World Congress of Soil Science, 1–6 August, Brisbane, Australia (published on DVD).

Kämpf, N., Schwertmann, U., 1983. Geothite and hematite in a climosequence in southern Brazil and their application in classification of kaolinitic soils. Geoderma 29, 27–39.

Lisiecki, L.E., Raymo, M.E., 2005. A Pliocene/Pleistocene stack of 57 globally distributed benthic oxygen-18 records. Paleoceanography 20 (PA1003), 1–17.

Mahaney, W.C., 1990. Ice on the Equator. Wm Caxton Press, Ellison Bay, Wisc.(386 pp.).

Mahaney, W.C., Fahey, B.D., 1988. Extractable Fe and Al in Late Pleistocene and Holocene paleosols on Niwot Ridge, Colorado Front Range. Catena 15, 17–26.

Mahaney, W.C., Hancock, R.G.V., Sanmugadas, K., 1991. Extractable Fe–Al and geochemistry of Late Pleistocene paleosols in the Dalijia Shan, western China. J. Southeast Asian Earth Sci. 6, 75–82.

Mahaney, W.C., Vortisch, W., Barendregt, R.W., 1997. Relative age of loess and till in two Quaternary paleosols in Gorges Valley, Mount Kenya, East Africa. J. Quat. Sci. 12, 61–72.

Mahaney, W.C., Sanmugadas, K., Hancock, R.G.V., 1999. Extractable Fe and Al of soils in the Middle Teton chronosequence, western Wyoming, U.S.A. Z. Geomorphol. 43, 393–407.

Mahaney, W.C., Falen, A.L., Fosberg, M.A., Hancock, R.G.V., 2006. Later Pleistocene and Holocene soils in Mammoth Basin and Green River areas, Wind River Mountains, Wyoming. Z. Gletscherk. Glazialgeol. 39, 161–181.

Mahaney, W.C., Dohm, J.M., Kapran, B., Hancock, R.G.V., Milner, M.W., 2009. Secondary Fe and Al in Antarctic paleosols: correlation to Mars with prospect for the presence of life. Icarus 203, 320–330.

Mahaney, W.C., Kalm, V., Hancock, R.G.V., Michel, F., Kapran, B., 2010. Geochemistry and extractable Fe and Al in cold temperature soils of northwestern Siberia. J. Quat. Sci. 25, 178–179.

Mahaney, W.C., Barendregt, R.W., Villeneuve, M., Dostal, J., Hamilton, T.S., Milner, M.W., 2011. Late Neogene volcanics and interbedded palaeosols near Mount Kenya. In: Van Hinsbergen, D.J.J., Buiter, S.J.H., Torsvik, T.H., Gaina, C., Webb, S.J. (Eds.), The Formation and Evolution of Africa: A Synopsis of 3.8 Ga of Earth History. Geological Society, London, pp. 301–318.

Mahaney, W.C., Krinsley, D.H., Allen, C.C.R., Langworthy, K., Ditto, J., Milner, M.W., 2012. Weathering rind: archives of paleoenvironments on Mount Kenya, East Africa. Journal of Geology 120, 591–602.

Mahaney, W.C., Barendregt, R.W., Hamilton, T.S., Hancock, R.G.V., Tessler, D., Costa, P.J.M., 2013a. Stratigraphy of the Gorges Moraine System, Mount Kenya: paleosol record and paleoclimate. J. Geol. Soc. http://dx.doi.org/10.1144/jgs2012-079.

Mahaney, W.C., Krinsley, D.H., Allen, C.C.R., 2013b. Biomineralization of weathered rock rinds: examples from the lower Afroalpine zone on Mount Kenya. Geomicrobiology 30, 1–11.

Martini, J.A., 1970. Allocation of cation exchange capacity to soil fractions in seven surface soils from Panama and the application of a cation exchange factor as a weathering index. Soil Sci. 109, 324–331.

McKeague, A., Day, J., 1966. Dithionite and oxalate extractable Fe and Al as aids in differentiating various classes of soils. Can. J. Soil Sci. 46, 13–22.

Mehra, O.P., Jackson, M.L., 1960. Iron oxide removal from soils and clays by a dithionite–citrate system buffered with sodium bicarbonate. National Conf. on Clays and Clay Minerals, 1958. Pergamon, London, pp. 317–327.

National Soil Survey Center (NRCS), 2004. Soil Survey Laboratory Methods Manual. In: Burt, R. (Ed.), Soil Survey Investigations Report no. 42, version 4.0. U.S.D.A. (700 pp.).

Nelson, F.E., Barendregt, R.W., Villeneuve, M., 2009. Stratigraphy of the Fort Selkirk volcanogenic complex in Central Yukon and its paleoclimatic significance: Ar/Ar and paleomagnetic data. Can. J. Earth Sci. 46, 381–401.

Oyama, M., Takehara, H., 1970. Standard Soil Color Charts. Japan Research Council for Agriculture, Forestry and Fisheries.

Pai, C.-W., Wang, M.-K., Shuang, S.-Y., King, H.-B., 2004. Free and non-crystalline Fe-oxides to total iron concentration ratios correlated with ^{14}C ages of three forest soils in Central Taiwan. Soil Sci. 169, 582–589.

Parfitt, R.L., Childs, C.W., 1988. Estimation of forms of Fe and Al: a review and analysis of contrasting soils by dissolution and Moessbauer methods. Aust. J. Soil Res. 26, 121–144.

Peech, M.L., Alexander, T., Dean, L.A., Reed, J.F., 1947. Methods of soil analyses for soil fertility investigations. Circ, 757. USDA, Washington, D.C. 25.

Ries, A.C., Vernacombe, J.R., Price, R.C., Shackleton, R.M., 1992. Geochronology and geochemistry of the rocks associated with a late proterozoic ophiolite in West Pokot, NW Kenya. J. Afr. Earth Sci. 14, 25–35.

Rogers, N.W., 2006. Basaltic magmatism and the geodynamics of the East African Rift system. In: Yirgu, G., Ebinger, G., Maguire, C.J., P.K.H. (Eds.), The Afar Volcanic Province within the East African Rift System. Special Publication, 259. Geological Society of London, London, pp. 77–93.

Schluter, Thomas, 1997. Geology of East Africa (with contributions by Craig Hampton). Science Publishers, Stuttgart (484 pp.).

Schoeneberger, P.J., Wysocki, D.A., Benham, E.C., Broderson, W.D. (Eds.), 2002. Field book for describing and sampling soils, Version 2.0. Natural Resources Conservation Service, National Soil Survey Center, Lincoln, NE.

Schollenberger, C.J., Simon, R.H., 1945. Determination of exchange capacity and exchangeable bases in soils—ammonium acetate method. Soil Sci. 59, 13–24.

Schülli-Maurer, I., Sauer, D., Stahr, K., Sperstad, R., Sorensen, R., 2007. Soil formation in marine sediments and beach deposits of southern Norway: investigations of soil chronosequences in the Oslofjord region. Rev. Mex. Cienc. Geol. 24, 237–246.

Soil Classification Working Group, 1998. The Canadian System of Soil Classification, Agriculture and Agri-Food Canada Publication 16463rd ed. (187 pp.).

Soil Survey Staff, 2010. Keys to Soil Taxonomy, 11th ed. U.S. Gov. Printing Office, Washington, D.C.

Trauth, M.H., Maslin, M.A., Deino, A., Strecker, M.R., 2005. Late Cenozoic moisture history of East Africa. Science 309, 2051–2053.

Veldkamp, A., Buis, E., Wijbrans, J.R., Olago, D.O., Boshoven, E.H., Marée, M., Van den Berg van Saparoea, R.M., 2007. Late Cenozoic fluvial dynamics of the River Tana, Kenya, an uplift dominated record. Quat. Sci. Rev. 26, 2897–2912.

Vernacombe, J.R., 1983. A proposed continental margin in the Precambrian of Western Kenya. Geol. Rundsch. 72, 663–670.

Walker, A., 1983. The effects of magnetite on oxalate- and dithionite-extractable iron. Soil Sci. Soc. Am. J. 47, 1022–1025.

Whittig, L.D., 1965. X-ray diffraction techniques for numerical identification and mineralogical composition. In: Black, C.A. (Ed.), Methods of Soil Analysis. American Society of Agronomy, Madison, Wisc., pp. 671–696.